Beyond the Tradeoff: Dynamic Selectivity in Ionic Transport and Current Rectification

Anthony R. Poggioli,[†,‡] Alessandro Siria,[†,‡] and Lydéric Bocquet*[,†,‡]

[†]Laboratoire de Physique Statistique, Ecole Normale Supérieure, Paris 75005, France
[‡]Centre National de la Recherche Scientifique, Paris 75005, France

ABSTRACT: Traditionally, ion selectivity in nanopores and nanoporous membranes is understood to be a consequence of Debye overlap, in which the Debye screening length is comparable to the nanopore radius somewhere along the length of the nanopore(s). This criterion sets a significant limitation on the size of ion-selective nanopores, as the Debye length is on the order of 1−10 nm for typical ionic concentrations. However, the analytical results we present here demonstrate that surface conductance generates a dynamical selectivity in ion transport, and this selectivity is controlled by so-called Dukhin, rather than Debye, overlap.

The Dukhin length, defined as the ratio of surface to bulk conductance, reaches values of hundreds of nanometers for typical surface charge densities and ionic concentrations, suggesting the possibility of designing large-nanopore (10−100 nm), high-conductance membranes exhibiting significant ion selectivity. Such membranes would have potentially dramatic implications for the efficiency of osmotic energy conversion and separation techniques. Furthermore, we demonstrate that this mechanism of dynamic selectivity leads ultimately to the rectification of ionic current, rationalizing previous studies, showing that Debye overlap is not a necessary condition for the occurrence of rectifying behavior in nanopores.
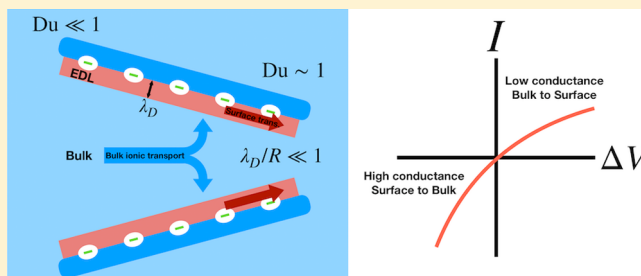
INTRODUCTION

Ionic and water transport in nanometric confinement has been an active topic of research for two decades,[1] with practical applications to macro-/biomolecular analysis,[2−5] energy generation,[1,6−10] and desalination.[1,11] Of particular interest is understanding via what mechanisms and under what conditions one may obtain nonlinear responses of fluxes (charge, solute mass, and solvent mass) to external forcings (voltage, pressure, and concentration difference). A detailed theoretical understanding of such nonlinear transport processes is a necessary first step in designing exotic tailored nanopore and membrane functionalities.[12] The most well-known example of such a nonlinear response is ionic current rectification (ICR), in which the ionic currents driven through nanopores by applied voltages of equal magnitude and opposite sign are found to be of unequal magnitude, in analogy to solid-state semiconductor diodes.[1,13] ICR has been extensively studied experimentally and via continuum simulations, as in refs,[14−26] though comparatively few studies have examined the phenomenon analytically.[11,19,27] Experimentally, it is found that ICR may be induced by unequal reservoir concentrations,[28] asymmetric geometries,[15,19,25,29−31] or asymmetric surface charge distributions.[18,26,32]

ICR is generally understood to be a consequence of the accumulation or depletion of ionic concentration induced by a gradient in ion selectivity along the length of a nanopore.[33] The key parameter controlling the local selectivity is accordingly the ratio of the local Debye length λ_D to the local nanopore radius R. The Debye length is defined as

$$\lambda_D \equiv \sqrt{\frac{\epsilon_r \epsilon_0 k_B T}{e^2 \sum_j z_j^2 c_j}} \tag{1}$$

where ϵ_r and ϵ_0 are, respectively, the relative dielectric permittivity of the solvent and the vacuum permittivity, k_B is the Boltzmann constant, T is the thermodynamic temperature, e is the elementary charge, z_j is the valence of the jth ionic species, and c_j is the concentration of the jth ionic species. This length scale characterizes the thickness of the diffuse layer of net ionic charge that forms in the vicinity of charged surfaces.[1] As the diffuse layer must counterbalance the surface charge, a region of strong Debye layer overlap, $\lambda_D/R \gtrsim O(1)$, should be highly selective to counterions, while a region of weak Debye overlap, $\lambda_D/R \ll 1$, should be essentially nonselective.

Debye overlap has significant consequences for ionic transport through the pore. In order to illustrate the underlying physical mechanisms, consider a conical nanopore with a uniform surface charge density, as discussed in ref 33. When $\lambda_D/R \gtrsim O(1)$ in the vicinity of the nanopore tip, a Donnan equilibrium between the tip and the connected reservoir forms, and this region is highly selective to (positive) counterions.

The tip is then a region of increased transference of cations and suppressed transference of anions. Thus, when an external electric field is directed from the (nonselective) base to the (highly selective) tip, both cations and anions pass from regions of relatively lower to relatively higher transference, and the result at steady state is a depletion of ionic concentration in the nanopore interior. The depletion of charge carriers results in a decrease of the local electrophoretic conductivity and corresponds to the low conductance (reverse-bias) diode state. On the other hand, if the direction of the applied field is inverted, both ionic species pass from regions of relatively high to relatively low transference, resulting in an accumulation of ionic concentration. This accumulation of charge carriers likewise results in a high conductance (forward-bias) state. Altogether, the criterion $\lambda_D/R \gtrsim 1$ is expected to be a prerequisite to observe nonlinear ionic transport, and in particular ICR. The mechanism of concentration accumulation and depletion in ICR has since been extensively corroborated numerically[14−18,21−24,27,34] and experimentally.[29]

However, recent studies have indicated not only that the parameter λ_D/R fails to predict the occurrence or strength of rectification, but also that significant rectification may be obtained even when the Debye length is 1 to 3 orders of magnitude smaller than the minimum nanopore radius.[12,21−25,31,35,36] To our knowledge, no consistent alternative criterion has been proposed to predict the occurrence of ICR. Furthermore, while there have been many numerical simulations of ICR within the Poisson−Nernst−Planck (PNP) or PNP−Stokes framework, few studies have offered a detailed theoretical analysis of the phenomenon, and these studies are typically confined to quite specialized scenarios, for example, ref [11].

In this paper, we demonstrate that the nanopore selectivity is not determined by the relative value of the Debye length λ_D compared to the pore radius, but rather by a dynamic criterion related to the relative magnitudes of the surface and bulk ionic conductions. This introduces the so-called Dukhin length, l_{Du}, defined as the ratio of the surface conductivity to the bulk conductivity in the nanopore.[1] The Dukhin length can be adequately rewritten in terms of the charge density on the pore surface, σ, as $l_{Du} = (|\sigma|/e)/c$, with c the bulk salt concentration.[1] A dimensionless Dukhin number is accordingly introduced as

$$Du \equiv \frac{l_{Du}}{R} \equiv \frac{|\sigma|}{ecR} \tag{2}$$

The Dukhin length approaches values of hundreds of nanometers for typical surface charges in the range of 10−100 mC m^{-2} and concentrations in the range of 0.1−1 mM, 1 to 2 orders of magnitude larger than the corresponding Debye lengths. Written in terms of the surface charge density (eq 2), we note that the criterion $Du > 1$ for substantial selectivity/ICR is equivalent to the criterion $|\sigma| > ecR$ noted by some authors.[30,37,38]

As we demonstrate below, substantial ionic selectivity may be obtained when the nanopore radius is comparable to the Dukhin length. This is consistent with numerical results indicating substantial ion selectivity may be obtained in highly charged pores with radii much larger than the Debye length,[37] and it is in stark contrast to traditional ion-selective membranes, which typically have subnanometric pore sizes.[6] We term this mechanism dynamic selectivity, in contrast to the

"thermodynamic" picture of ionic selectivity based on Debye overlap and the formation of a Donnan equilibrium at the ends of the nanopore, for example, refs.[1,33,39] The possibility of obtaining significant selectivity for large (10−100 nm) pores may have significant implications for, for example, osmotic energy generation; we will discuss this point in more detail below.

Furthermore, we will show below that a gradient in the local Dukhin number along the length of the nanopore results in a repartitioning of the fraction of the ionic transport carried in the nonselective bulk and in the highly selective Debye layer. It is this repartitioning, rather than Debye overlap and the formation of a local Donnan equilibrium at one end of the nanopore, that results in ICR.

Our starting point will be the derivation of one-dimensional transport equations from a radial integration of the axisymmetric PNP equations in the limit that $\lambda_D/R \ll 1$ but $Du \approx 1$; we focus on this limit as we are particularly interested in rationalizing those experimental[12,22,25,31,35,36] and numerical[12,21,23,24,37] results, indicating that substantial rectification and selectivity may occur even when $\lambda_D/R \ll 1$. We note that reanalysis of the data reported in the literature corroborates the assertion that significant rectification occurs when $Du \approx 1$, irrespective of the value of λ_D/R; this is discussed below.

From these transport equations, we are able to derive a simple implicit expression for the current−voltage (IV) response in a concentration diode. To our knowledge, this is the first time such a solution has been presented. Additionally, we will give numerical solutions of these transport equations for a geometric diode (rectification induced by an asymmetric, continuously varying radius) and a charge diode (rectification induced by an asymmetric, continuously varying surface charge density distribution). These solutions will directly illustrate the key role of the local Dukhin number and the mechanism of dynamic selectivity in ICR. Finally, we derive analytical expressions for general limiting conductances directly from the transport equations that will be useful in estimating, for example, surface charge densities from rectified IV curves.

■ THEORY

1D Transport Equations in the Absence of Debye Overlap. In this section, we derive one-dimensional transport equations for the electrostatic potential and total ionic concentration at the nanopore centerline from the axisymmetric PNP equations. Our derivation relies on the geometric constraint, $R_0/l \ll 1$, where R_0 is a scale of the radial extent of the nanopore, and l is a characteristic scale of variation of the nanopore geometry. This slowly varying approximation implies that a Poisson−Boltzmann (PB) equilibrium holds locally on each cross section.[7,40] As we intend to demonstrate that the Dukhin number is the principal parameter controlling selectivity and ICR, and that ICR may occur even in the absence of Debye overlap anywhere along the length of the nanopore, we focus on the regime that $\lambda_D/R \ll 1$. There is no Debye overlap in the center of the nanopore so that the electrolyte there is electroneutral, and we may partition the ionic concentrations and electrostatic potential as follows[40]

$$c_{\pm}(x, r) = \frac{c_0(x)}{2} + \delta c_{\pm}(x, r) \tag{3}$$

$$\phi(x, r) = \phi_0(x) + \delta\phi(x, r) \tag{4}$$

where $c_0(x) \equiv c(x,0)$ is the value of the total ionic concentration, $c \equiv c_+ + c_-$ at the nanopore centerline ($r = 0$), $\phi_0(x) \equiv \phi(x,0)$ is the electrostatic potential at the nanopore centerline, and $\delta c_\pm(x,r)$ and $\delta\phi(x,r)$ are the radial deviations in the ionic concentrations and electrostatic potential, respectively, induced by the formation of a screening Debye layer in the vicinity of the nanopore wall. In eq 3, we have assumed a symmetric (z/z) salt. In what follows, we will assume a monovalent (1:1) salt in which the cation and anion have identical mobility and diffusion coefficients.

With this notation and these assumptions, the steady-state PNP equations reduce to

$$j_\pm = -D\left(\frac{\partial c_\pm}{\partial x} \pm \frac{e}{k_B T}c_\pm\frac{\partial\phi}{\partial x}\right) \tag{5}$$

$$\frac{d}{dx}\left(2\pi\int_0^R dr\, r j_\pm\right) \equiv \frac{dJ_\pm}{dx} = 0 \tag{6}$$

$$\epsilon_r\epsilon_0\frac{1}{r}\frac{\partial}{\partial r}\left(r\frac{\partial\delta\phi}{\partial r}\right) + n_c \approx \epsilon_r\epsilon_0\frac{\partial^2\delta\phi}{\partial Z^2} + n_c = 0 \tag{7}$$

$$c = c_0\cosh\left(\frac{e\delta\phi}{k_B T}\right) \tag{8}$$

and

$$n_c = -ec_0\sinh\left(\frac{e\delta\phi}{k_B T}\right) \tag{9}$$

where D is the diffusion coefficient, e is the elementary charge, k_B is the Boltzmann constant, T is the thermodynamic temperature, R is the local nanopore radius, ϵ_r (≈ 80 for water at room temperature) is the relative permittivity of the solvent, ϵ_0 is the vacuum permittivity, and $n_c \equiv e(c_+ - c_-)$ is the ionic charge density. In eq 7, we have neglected the portion of the radial gradient induced by the curvature of the nanopore wall as it is suppressed by a factor $\lambda_D/R \ll 1$ relative to ∂_r^2, and we have introduced the coordinate $Z \equiv R - r$. Equation 5 is the ionic flux density along the flow (x) direction; eq 6 is the cross-sectionally integrated continuity equation at the steady state; eq 7 is the Poisson equation, retaining only the radial component of the electric field divergence in accordance with the slowly varying approximation; and eqs 8 and 9 are the distributions of the total ionic concentration and ionic charge density obtained from the Boltzmann distribution, applied on the assumption of a slowly varying geometry. Finally, we have neglected advection as it is not expected to affect our conclusions,[14,37] and such an approach allows for tractable analytical derivations.

Before continuing, we introduce dimensionless rescaled variables, as listed in Table 1; we have rescaled the x-coordinate by the total nanopore length L and the surface charge σ by a reference magnitude $|\sigma_{ref}|$, and we have introduced $\bar{c}$, the average of the reservoir concentrations, as a scale of ionic concentration in the nanopore. In what follows, we will take the reference surface charge magnitude $|\sigma_{ref}|$ to be either the magnitude of the surface charge density when it is uniform, or the maximum surface charge magnitude when the surface charge density is nonuniform. We further recast eqs 5 and 6 in terms of the rescaled solute flux $J \equiv J_+ + J_- \equiv \int dA j$ and ionic current $I \equiv J_+ - J_- \equiv \int dA i$. With these modifications, the governing equations become

Table 1. Independent and Dependent Variables and Their Rescaled Dimensionless Counterparts

quantity	variable	rescaled
position	x	$x \to Lx$
radius	R	$R \to R_{min}R$
concentration	c	$c \to \bar{c}c$
ionic charge density	n_c	$n_c \to e\bar{c}n_c$
electrostatic potential	ϕ	$\phi \to (k_B T/e)\phi$
electrochem. potential	$\mu_\pm$	$\mu_\pm \to k_B T\mu_\pm$
flux density	$j_\pm$	$j_\pm \to (D\bar{c}/L)j_\pm$
surface charge	σ	$\sigma \to |\sigma_{ref}|\sigma$
conductance	G	$G \to (R_{min}^2/L)(e^2 D/k_B T)\bar{c}$

$$j = -\left(\frac{\partial c}{\partial x} + n_c\frac{\partial\phi}{\partial x}\right) \tag{10}$$

$$i = -\left(\frac{\partial n_c}{\partial x} + c\frac{\partial\phi}{\partial x}\right) \tag{11}$$

$$\frac{dJ}{dx} = \frac{dI}{dx} = 0 \tag{12}$$

$$\left(\frac{\lambda_D^{ref}}{R_0}\right)^2\frac{\partial^2\delta\phi}{\partial Z^2} + n_c = 0 \tag{13}$$

$$c = c_0\cosh(\delta\phi) \tag{14}$$

and

$$n_c = -c_0\sinh(\delta\phi) \tag{15}$$

where we have introduced a reference Debye length $\lambda_D^{ref} \equiv \sqrt{k_B T\epsilon_r\epsilon_0/e^2\bar{c}}$, defined in terms of the mean reservoir concentration $\bar{c}$.

We differentiate eq 14 (15) with respect to x, insert the result into eq 10 (11), and integrate on the cross section to obtain

$$\frac{J}{\pi R^2} = -\frac{dc_0}{dx} - \frac{\langle\delta c\rangle}{c_0}\frac{dc_0}{dx} - \frac{\langle n_c\rangle}{c_0}c_0\frac{d\phi_0}{dx} \tag{16}$$

and

$$\frac{I}{\pi R^2} = -c_0\frac{d\phi_0}{dx} - \frac{\langle n_c\rangle}{c_0}\frac{dc_0}{dx} - \frac{\langle\delta c\rangle}{c_0}c_0\frac{d\phi_0}{dx} \tag{17}$$

where $\langle\rangle \equiv A^{-1}\int dA$ denotes a cross-sectional average. The integral of the charge density is set by the condition of local electroneutrality, a necessary consequence of a local PB equilibrium; the integral of δc may be evaluated using the PB equilibrium theory (eqs 13−15) in the limit $\lambda_D/R \ll 1$. The condition of local electroneutrality requires that

$$\frac{\langle n_c\rangle}{c_0} = -2Du_{ref}\frac{\sigma}{Rc_0} \equiv -2Du(x) \tag{18}$$

where $Du_{ref} \equiv |\sigma_{ref}|/e\bar{c}R_0$ is a reference Dukhin number, and $Du(x)$ is the local Dukhin number. We note that Du_{ref} is defined to be always positive, but $Du(x)$ carries the sign of the local surface charge density. The integral of δc can be evaluated using eqs 13−15. The result is

$$\frac{\langle \delta c \rangle}{c_0} = 4 \frac{\lambda_D}{R_0 R} \left\{ \sqrt{\left[\frac{Du}{2(\lambda_D/R_0 R)} \right]^2 + 1} - 1 \right\} \tag{19}$$

where Du is the local value of the Dukhin number, and $\lambda_D(x) \equiv \lambda_D^{ref}/\sqrt{c_0(x)}$ is the local Debye length. In the limit $(\lambda_D/R_0 R)/Du \to 0$, this reduces to

$$\frac{\langle \delta c \rangle}{c_0} = 2|Du(x)| \tag{20}$$

We will consider this limit in developing an analytical solution for the concentration diode below, as we are most interested in the scenario that there is no Debye overlap $(\lambda_D(x)/R(x)R_0 \ll 1$ everywhere), but the Dukhin number is of order one $(Du(x) \approx 1$ somewhere). In this case, the transport equations, eqs 16 and 17, become

$$\frac{J}{\pi R^2} = -\left[\frac{dc_0}{dx} + 2|Du(x)|\frac{dc_0}{dx} - 2Du(x)c_0\frac{d\phi_0}{dx} \right] \tag{21}$$

and

$$\frac{I}{\pi R^2} = -\left[c_0 \frac{d\phi_0}{dx} - 2Du(x)\frac{dc_0}{dx} + 2|Du(x)|c_0\frac{d\phi_0}{dx} \right] \tag{22}$$

where I and J are of course constant along the length of the nanopore (eq 12). It is useful to distinguish between those terms in eqs 21 and 22 that arise from transport outside of the Debye layer (bulk transport) and those arising from transport within the Debye layer (surface transport). In the equation for the solute flux (eq 21), the terms represent, from left to right, bulk diffusion, surface diffusion, and surface electrophoretic mass transport. In the equation for the ionic current (eq 22), the terms represent bulk electrophoretic current, surface charge diffusion, and surface electrophoretic current. We see that the local Dukhin number, which sets the cross-sectionally averaged ionic charge (eq 18), as well as the cross-sectionally averaged excess concentration when $\lambda_D/R_0 R \ll Du$ (eq 20), determines the ratio of surface to bulk transport. Motivated by this observation, we quantify the ratio of the surface transport to the total transport by the following surface transport ratio (STR)

$$STR(x) \equiv \frac{2|Du(x)|}{1 + 2|Du(x)|} \tag{23}$$

We see immediately that the partitioning of the transport into surface and bulk components adjusts along the length of the nanopore and is controlled locally by the Dukhin number. In the case that there is a large asymmetry in the Dukhin number on either end of the nanopore, this can result in a substantial repartitioning of the transport in the nanopore interior, the consequences of which will be explored in the following sections.

An illustrative form of eqs 21 and 22 is obtained by introducing the definition of the local Dukhin number, eq 18, and defining the coion and counterion fluxes $J_{co/count} \equiv (J \pm SI)/2$ and electrochemical potentials $\mu_{co/count} \equiv \ln(c_0/2) \pm S\phi$. In the preceding definition, $S \equiv \text{sign}(\sigma)$ is the sign of the surface charge. Inserting these definitions into eqs 21 and 22, we obtain

$$\frac{J_{co}}{\pi R^2} = -\frac{c_0}{2}\frac{d\mu_{co}}{dx} \tag{24}$$

$$\frac{J_{count}}{\pi R^2} = -\left(\frac{c_0}{2} + 2Du_{ref}\frac{|\sigma|}{R} \right)\frac{d\mu_{count}}{dx} \tag{25}$$

Note that we have implicitly assumed in deriving these equations from eqs 21 and 22 that the sign of the surface charge S does not change along the length of the nanopore. If the sign of the surface charge does change at one (or several) points along the length of the nanopore, eqs 24 and 25 may be applied in each region delineated by a discontinuity in $S(x)$, matching c_0 and ϕ_0 at each discontinuity. (More about the proper boundary conditions for eqs 21/24 and 22/25 will be said below.)

In eqs 24 and 25, we recognize $c_0/2$ as the concentration of both coions and counterions at the nanopore centerline. Further, in eq 25, we recognize $2Du_{ref}|\sigma|/R$ as the additional concentration accumulated in the Debye layer (eq 20). The term $2Du_{ref}|\sigma|/R \times d\mu_{count}/dx$ in eq 25 represents the entirety of the surface transport in the nanopore; this indicates that coions are perfectly excluded from the Debye layer in the limit $\lambda_D/R \ll Du$ (R dimensioned). This will be shown to be the case from PB equilibrium theory and the condition of local equilibrium below.

We will employ eqs 21 and 22 below to develop an implicit analytical solution for the current−voltage (IV) relationship in a concentration diode.

Dynamic Selectivity. As noted above, in the slowly varying limit $(R_0/l \ll 1)$ considered here, the ionic concentration profiles on the cross section deviate negligibly from those predicted by the PB equilibrium theory. Thus, we may apply this equilibrium theory to determine how the ionic selectivity on the cross section is influenced by Debye overlap (λ_D/R) and the Dukhin number. Using eqs 18 and 19, we determine the cross-sectionally averaged total concentration, $\langle c \rangle = \langle \delta c \rangle + c_0$, and the cross-sectionally averaged counterion concentration, $\langle c_{count} \rangle = (\langle c \rangle + |\langle n_c \rangle|)/2$. We take the ratio $\langle c_{count} \rangle / \langle c \rangle$ as a metric of selectivity; this parameter ranges between 1/2, indicating that the total average concentration is equally partitioned between coions and counterions and the nanopore is locally nonselective, and unity, indicating that the entirety of the average concentration is due to counterions, and the nanopore is therefore perfectly selective. We find that, in the range $0 < \lambda_D/R < 2(10^{-1})$, the nanopore selectivity is strongly influenced by the local Dukhin number in the range $10^{-1} < Du < 10^1$ (Figure 1). In comparison, the influence of λ_D/R on selectivity for this range of λ_D/R is substantially less pronounced.

From Equilibrium to Dynamical Selectivity. As noted above, eqs 24 and 25 suggest that the Debye layer is perfectly selective in the limit $(\lambda_D/R)/Du \to 0$. This can be confirmed as follows: for a monovalent ionic species, the deviations in the counterion (coion) concentration from the centerline potential in the Debye layer are related to δc and n_c by $\delta c_{count} = (\delta c + |n_c|)/2$ $(\delta c_{co} = (\delta c - |n_c|)/2)$. With these expressions and eqs 18 and 20, we find that $\langle \delta c_{count} \rangle = 2|Du|c_0$ and $\langle \delta c_{co} \rangle = 0$, confirming that the Debye layer is indeed perfectly selective in this limit.

An upper limit on the selectivity induced by Debye overlap may be obtained by considering the selectivity of the nanopore entrance/exit in the limit $\lambda_D/R \to \infty$. In this case, we may impose electrochemical equilibrium across the junction
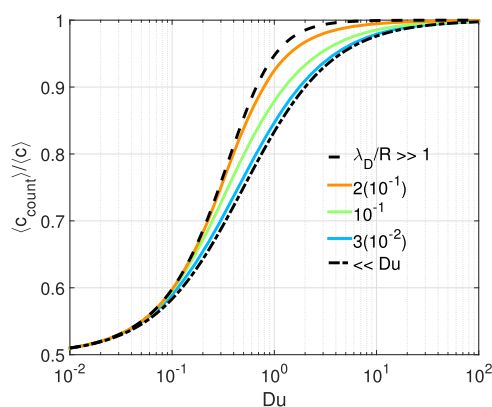
Figure 1. Ratio of the cross-sectionally averaged counterion concentration to the cross-sectionally averaged total concentration, a metric of the nanopore selectivity, as a function of Dukhin number. The lines are colored according to λ_D/R, as indicated in the legend. The dashed (dot-dashed) line indicates the curve obtained in the limit $\lambda_D/R \to \infty$ ($\to 0$).

between the interior of the nanopore and the reservoir and local electroneutrality on either side.[1] The ratio of counterion to total concentration is then found to be[1]

$$\frac{\langle c_{count} \rangle}{\langle c \rangle} = \frac{\sqrt{\left(\frac{1}{2}\right)^2 + |Du|^2} + |Du|}{\sqrt{1 + (2|Du|)^2}} \qquad (26)$$

This upper limit exceeds the selectivity obtained above for $\lambda_D/R = 2(10^{-1})$ only slightly (Figure 1), indicating that the nanopore selectivity rapidly saturates for values of $\lambda_D/R \gtrsim 1/5$.

A lower limit, valid when $\lambda_D/R \ll Du$, is obtained via eqs 18 and 20. In this case, we find

$$\frac{\langle c_{count} \rangle}{\langle c \rangle} = \frac{1}{2}\left(1 + \frac{2|Du|}{1 + 2|Du|}\right) \equiv \frac{1}{2}(1 + STR) \qquad (27)$$

where in the second equality we have made use of eq 23. Equation 27 shows the deep connection between transport and selectivity and can be made more intuitive as follows. As shown above, the Debye layer in this limit is perfectly selective, so that the ratio of the counterion concentration to total concentration is unity. As always, the bulk is perfectly nonselective, so that the ratio there is 1/2. As the STR is the ratio of surface transport to total transport, the ratio of bulk-to-total transport is $1 - STR$, and we may estimate the total selectivity on the cross section based on the partitioning of the ionic transport as

$$\underbrace{\frac{1}{2} \times (1 - STR)}_{bulk} + \underbrace{1 \times STR}_{surface} = \frac{1}{2}(1 + STR)$$

We thus recover the result given in eq 27. This result illustrates that it is the selectivity in the bulk and surface weighted by the dynamic partitioning of the ionic transport that controls local selectivity.

Together, the upper and lower limits on selectivity (eqs 26 and 27, respectively) define an envelope of selectivity variation with λ_D/R (Figure 1). The conclusion of these results is apparent: the principal parameter controlling nanopore selectivity is not λ_D/R but the local Dukhin number. This result may be understood as follows: when λ_D/R is small, the local Dukhin number controls both the fraction of the transport in the Debye layer (eq 23), and the selectivity of

the Debye layer (eq 27). A large value of Du means that the majority of the ionic flux is carried within the Debye layer, and that this region is highly selective. Thus, even though the unselective bulk region takes up the majority of the cross section, the majority of the transport must pass through the highly selective but relatively small Debye layer. As this process is controlled by the local Dukhin number and the local partitioning of ionic currents, both of which adjust dynamically, we refer to it as dynamic selectivity.

On the other hand, when λ_D/R is large, a significant surface charge (as quantified by the Dukhin number) must still be present to draw counterions into (and exclude coions from) the nanopore and thus render the nanopore highly selective. This is indicated in the Donnan result for the selectivity (eq 26). All together, the result is the dominance of the local Dukhin number in determining the local nanopore selectivity (Figure 1).

These results suggest that a nanopore may exhibit significant selectivity when the pore size is comparable to the Dukhin length. As noted above, the Dukhin length reaches hundreds of nanometers for typical ionic concentrations (0.1−1 mM) and surface charge densities (10−100 mC m^{-2}). This is in strong contrast to traditional ion-selective membranes, which have typically subnanometric pore sizes,[6] and indeed to the typical picture of ion selectivity as occurring only in the presence of strong Debye overlap ($\lambda_D/R \gg 1$).[1]

We explore this idea by examining the ion selectivity under an applied concentration difference and voltage in a uniform nanopore and under an applied voltage in a conical nanopore.

Transport and Dynamic Selectivity. We first consider a nanopore of uniform negative surface charge density σ and constant radius R connecting a left reservoir of concentration c_L and applied voltage ΔV to a grounded right reservoir of concentration $c_R \leq c_L$ (Figure 2, inset). We anticipate here some of the results derived later in order to illustrate the concept of dynamic selectivity.
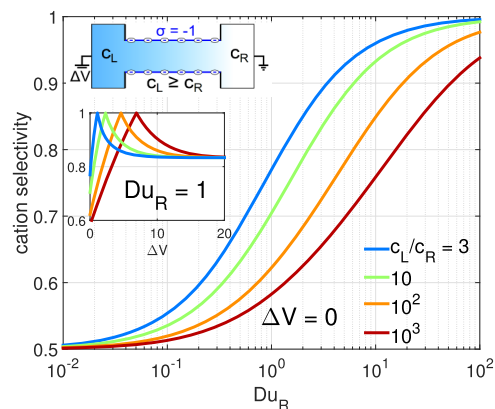

Figure 2. Cation selectivity for the diffusive flux in the absence of an applied voltage ($\Delta V = 0$) as a function of the larger imposed Dukhin number Du_R corresponding to the smaller reservoir concentration c_R. The curves are colored according to the corresponding value of c_L/c_R, as indicated in the legend. The fluxes are calculated for a nanopore of uniform negative surface charge density and constant radius, as indicated in the schematic in the upper left. The inset shows the selectivity as a function of voltage applied to the reservoir containing the larger concentration, c_L, and for a fixed value of $Du_R = 1$. The curves are colored according to c_L/c_R, as in the main panel, and the voltage is rescaled according to the thermal voltage $k_B T/e \approx 25$ mV.

As detailed below, we may solve the transport equations, eqs 21 and 22, to obtain an implicit algebraic solution for the ionic current and solute flux (eqs 35 and 36), from which we calculate the ionic flux $J_\pm \equiv (J \pm I)/2$ and the ion selectivities

$$\mathcal{S}_\pm \equiv \frac{|J_\pm|}{|J_+| + |J_-|} \tag{28}$$

Note from the above definition that the counterion selectivity will fall between 1/2 and 1, while the coion selectivity will fall between 0 and 1/2, such that $\mathcal{S}_+ + \mathcal{S}_- = 1$.

We show the results of a calculation of the cation (counterion) selectivity in a uniform nanopore under an applied concentration difference in Figure 2. The results are colored according to concentration ratio $c_L/c_R > 1$ and are plotted against the maximum Dukhin number $Du \equiv R|\sigma|/ec_R R$ imposed at the right end of the nanotube and corresponding to the smaller reservoir concentration c_R. We see that for moderate concentration ratios ($c_L/c_R \leq 10$), a maximum Dukhin number Du_R of order one results in selectivities of ~70−80%.

In the inset of Figure 2, we show the cation selectivity as a function of applied voltage ΔV, again colored according to concentration ratio c_L/c_R, and at a fixed $Du_R = 1$. We recall that the voltage is applied in the high concentration reservoir; this corresponds to the reverse-bias (low conductance) state of the concentration diode. As we will see below, generically, ion selectivity is maximized in a diode when voltage is applied in the reverse-bias direction. Under an applied voltage, the anion flux is reduced and eventually shut down as the anion chemical potential differential $\Delta\mu_- = \ln(c_L/c_R) - \Delta V$ decreases and vanishes. This results in a rapid increase in the cation selectivity as small voltages are applied in the high concentration reservoir and a peak cation selectivity of 100% when $\Delta V = \ln(c_L/c_R)$ and $J_- = 0$. We see in the inset of Figure 2 that the cation selectivity saturates at a value that is independent of c_L/c_R as ΔV is increased above $\ln(c_L/c_R)$ and anions begin to flow from the right to the left reservoir. This saturation value is given by

$$\mathcal{S}_+(\Delta V \to +\infty) = \frac{1 + 4Du_{max}}{2 + 4Du_{max}} \tag{29}$$

where Du_{max} is the larger of the two Dukhin numbers imposed on either end of the nanopore; in this case, $Du_{max} = Du_R$. For the present case, $Du_R = 1$, and the saturation value of the cation selectivity is ~83%. These results suggest that the nanopore selectivity may be tuned with the application of small external applied voltages. (Note that ΔV is rescaled by $k_B T/e \approx 25$ mV such that the maximum plotted voltage in the inset of Figure 2 $\Delta V = 20$ corresponds to ~500 mV.)

While the zero-voltage selectivity is not as optimal as traditional ion-selective membranes, which have counterion selectivity ratios ~99%, this tradeoff is more than made up for by pore diameters that are 1−2 orders of magnitude larger.

Let us consider two prototypical situations in which such effects could be usefully harnessed. Reverse electrodialysis (RED) is one of a few proposed techniques for the conversion of the osmotic energy associated with the salinity contrast between fresh and saltwater to mechanical energy. This technique depends on ion-selective diffusive fluxes of the type discussed above and shown in Figure 2 across stacks of alternating cation- and anion-selective membranes. The principal limiting factor in commercialization of this process

is the low conversion efficiency engendered by the high membrane resistance due to the subnanometric pores in typical ion-selective membranes.[6] Our results suggest that this problem may be circumvented by using large-pore (10−100 nm) membranes with pore diameters and surface charges tailored to the operating concentrations such that a maximum Dukhin number of order one is achieved.

Another phenomenon of interest is traditional electrodialysis (ED), in which an electric field is applied across stacks of cation- and anion-selective membranes in order to separate ions from brackish source water. In this case, what is of interest is the selectivity of the ionic flux induced by an applied voltage in the absence of a concentration differential. To this end, we first consider as a benchmark the performance (both selectivity and conductance) of a uniform nanopore—that is, a nanopore with constant (negative) surface charge density and radius; we then compare this to the performance of a conical nanopore having a fixed length, surface charge density, and tip radius R_{tip}. That is, we hold the tip Dukhin number $Du_{tip} \equiv |\sigma|/ecR_{tip}$ fixed while increasing the ratio of base and tip radii $\alpha \equiv R_{base}/R_{tip}$ above unity. The scenario under consideration is sketched in an inset in Figure 3. Our goal in increasing the opening angle is to improve the conductance compared to the uniform nanopore without a great cost to the nanopore selectivity.
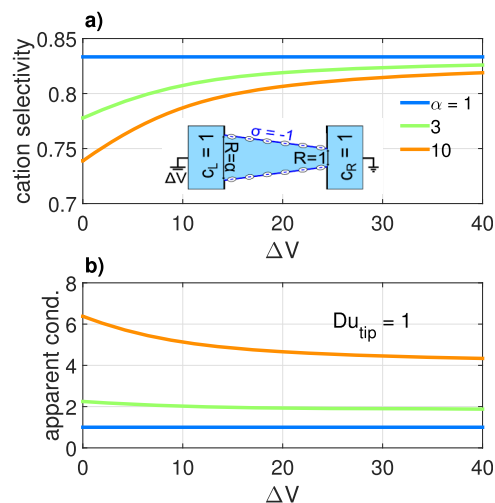

Figure 3. (a) Cation selectivity in a conical nanopore as a function of applied voltage and colored according to the ratio of base and tip radii $\alpha \equiv R_{base}/R_{tip} \geq 1$, as indicated in the legend. (b) Apparent conductance $G_{app} \equiv I/\Delta V$ normalized by the conductance of a uniform ($\alpha = 1$) nanopore (eqs 37−39) as a function of ΔV and colored according to $\alpha \equiv R_{base}/R_{tip}$, as in (a). The inset in panel a shows a schematic representation of the geometry considered here. All curves are calculated with a Dukhin number at the tip $Du_{tip} = 1$. The voltage is rescaled by the thermal voltage $k_B T/e \approx 25$ mV, and the variables indicated in the schematic are rescaled according to Table 1.

In the case of a uniform nanopore, the transport equations, eqs 21 and 22, are trivially solved for the conductance (given by eq 37−41) and the cation selectivity (given by eq 29 with $Du_{max} = Du_{tip}$). Note that in the case of a uniform nanopore, the cation selectivity is voltage-independent, as the Dukhin number is equal to Du_{tip} everywhere. This is indicated by the blue curves in Figure 3a, showing the cation selectivity as a function of voltage, and Figure 3b, showing the apparent conductance $G_{app} \equiv I/\Delta V$ normalized by the uniform nanopore conductance.

The influence of introducing a conical structure (i.e., increasing $\alpha \equiv R_{base}/R_{tip}$ above one) on the cation selectivity is shown in Figure 3a. In the vicinity of $\Delta V = 0$, the selectivity drops rapidly as α is increased, decreasing from the theoretical limit of ~83% (eq 29) to ~74% as α is increased from 1 to 10; however, as ΔV is increased, the selectivity again rapidly approaches the theoretical limit for large positive voltages. We note that the voltage is applied to the larger end of the conical nanopore; this again corresponds to the low conductance and high selectivity configuration of the diode. We see in Figure 3a that a voltage as small as ~1 V ($\Delta V = 40$) is enough to achieve a selectivity very nearly identical to the uniform nanopore selectivity.

We plot in Figure 3b the influence of increasing $\alpha \equiv R_{base}/R_{tip}$ on the apparent conductance. We see that the limiting apparent conductance for large positive applied voltages is substantially increased as α is increased. Increasing α to 3 is enough to approximately double the conductance, while $\alpha = 10$ results in a conductance that is more than four times larger than the uniform pore conductance. We will show below that the limiting conductance is related to the uniform nanopore conductance G_{uni} (eqs 37−41) by

$$G(\Delta V \rightarrow +\infty) = \frac{\alpha - 1}{\ln \alpha} G_{uni} \tag{30}$$

The results for a conical nanopore shown in Figure 3 and given in eqs 29 and 30 indicate that (1) substantial selectivity may be achieved in large (i.e., high conductance) uniform radius nanopores if the surface charge and pore radius is tailored to the operating concentrations such that $Du_{tip} \gtrsim 1$ and (2) the conductance may be even further enhanced by introducing a conical shape to the nanopore while holding the tip radius fixed. Together, these results suggest that, for example, desalination processes based on ED may be made substantially more efficient by using high surface charge, large, conical nanopores.

RESULTS

Role of Dynamic Selectivity in the Concentration Diode. In this section, we illustrate the principal role of the Dukhin number in ICR by developing an implicit expression for the IV relationship in a concentration diode using eqs 21 and 22. For a nanopore of uniform cross section, these equations are exactly valid cross-sectional integrations of the governing PNP equations in the limits $R/L \rightarrow 0$, $\lambda_D/R \rightarrow 0$, and $(\lambda_D/R)/Du \rightarrow 0$. Therefore, the fact that they produce rectified IV curves is strong evidence that $\lambda_D/R \gtrsim O(1)$ somewhere in the nanopore is not a necessary condition for the existence of ICR. As the rectification is fundamentally a consequence of the mechanism of dynamic selectivity outlined above, there is no fundamental mechanistic difference between ionic diodes induced by asymmetric geometry, differences in reservoir concentration, or (continuous) asymmetric surface charge profiles induced by, for example, differences in reservoir pH. In each case, the asymmetry induces an asymmetry in the Dukhin number $|Du| = |\sigma|/ecR$ across the nanopore, resulting in an asymmetry in the selectivity of the Debye layer and in the partitioning of the ionic transport between surface and bulk. We focus here on the concentration diode because we are able to derive an illustrative algebraic solution.

Fluxes Across a Concentration Diode. We consider here the same uniform nanopore configuration as described above

and shown schematically in the inset of Figure 2. The local Dukhin number along the length of the nanopore is given by

$$Du(x) = -\frac{Du_{ref}}{c} \tag{31}$$

where the reference Dukhin number $Du_{ref} \equiv |\sigma|/\bar{e}cR$ is defined in terms of the magnitude of the uniform surface charge density, the average of the two reservoir concentrations, and the uniform nanotube radius. We have omitted the subscript zero on the concentration, and we will continue to omit the subscript in what follows, recalling that the indicated total ionic concentrations and electrostatic potentials are centerline values.

We note that because the surface charge density and nanotube radius do not vary along the length of the nanopore the variation in the local Dukhin number is determined entirely by the variation in the local concentration. In addition to the reference Dukhin number, we introduce the local Dukhin numbers on the left and right of the nanotube, $Du_L \equiv Du_{ref}/c_L$, and $Du_R \equiv Du_{ref}/c_R$, respectively. We note that the ratio of Dukhin numbers $Du_R/Du_L \equiv c_L/c_R \geq 1$ is simply the ratio of reservoir concentrations. With these definitions, we can express the reference Dukhin number as

$$Du_{ref} = \frac{2}{Du_L^{-1} + Du_R^{-1}} \tag{32}$$

We will formulate our results below in terms of the maximum Dukhin number in the system, Du_R, corresponding to the minimum reservoir concentration, and the concentration ratio $Du_R/Du_L \equiv c_L/c_R$. Note that, while we do not impose particular values for the reservoir concentrations in our rescaled, dimensionless model, the concentration ratios considered here are consistent with the range of concentrations considered experimentally, typically between 0.1 mM and 1 M.

With the local Dukhin number given in eq 31, eqs 21 and 22 become

$$\frac{J}{\pi} = -\left[\frac{dc}{dx} + 2Du_{ref}\left(\frac{d\ln c}{dx} + \frac{d\phi}{dx}\right)\right] \tag{33}$$

and

$$\frac{I}{\pi} = -\left[c\frac{d\phi}{dx} + 2Du_{ref}\left(\frac{d\ln c}{dx} + \frac{d\phi}{dx}\right)\right] \tag{34}$$

Solving eqs 33 and 34 is a straightforward procedure, but before integrating, we must take care to ensure that we are imposing appropriate boundary conditions at the nanotube ends. This is a nontrivial question because the rapid variation in the local Dukhin number (from a nonzero value in the nanotube interior to zero in the reservoir) that occurs on either end of the nanotube means that the slowly varying approximation we have used to impose a local PB equilibrium breaks down.[11] In one-dimensional PNP-based models of nanopore ionic transport, this is typically taken into account by imposing continuity of the electrochemical potential $\mu_\pm = \ln c_\pm \pm \phi$ across the junction and local electroneutrality on either side.[1,11,15,16,27] This is justified as follows: the rapid variation in local geometry and consequently in the local Dukhin number results in localized deviations from equilibrium and electroneutrality and rapid variations in electrostatic potential and ionic concentrations. The scale of this adjustment region is given by the Debye length. (See the paper of Shockley[13] for an

extensive discussion of this point in the equivalent context of semiconductor physics.) Thus, in the limit $\lambda_D/L \to 0$, the adjustment region may be treated as a point discontinuity in the ionic concentrations and electrostatic potential. However, as the ionic flux densities $j_\pm = -c_\pm \partial_x u_\pm$ are proportional to the gradient of the electrochemical potential, the discontinuities in ionic concentration and electrostatic potential must be such that continuity of electrochemical potential is maintained, ensuring finite ionic fluxes. Outside of this adjustment region, the ions again locally equilibrate, and thus local electroneutrality is imposed on either side of the junction.

As we have already assumed a radially uniform electrochemical potential in locally applying a PB equilibrium, imposing continuity of the electrochemical potential between the uniform reservoir values and the values over the entire cross section in the nanotube interiors reduces to imposing electrochemical continuity between the reservoir and nanopore centerline. Furthermore, as the ionic charge vanishes at the nanopore centerline, imposition of electroneutrality there amounts to imposing $c_+^{int} = c_-^{int} = c_{int}/2$, where "int" indicates the value in the interior of the nanopore. Electrochemical continuity across the junction thus requires $\ln(c_{res}/2) \pm \phi_{res} = \ln(c_{int}/2) \pm \phi_{int}$, where "res" indicates the value in the reservoir. This condition is satisfied by imposing continuity of the ionic concentration and potential, $c_{res} = c_{int}$ and $\phi_{res} = \phi_{int}$, respectively.[7,40]

We note that (1) this still corresponds to finite discontinuities in the ionic concentrations and electrostatic potential within the Debye layer, and (2) there would be a discontinuity in centerline concentrations and electrostatic potential in the case of Debye overlap, as the ionic charge density would no longer vanish at the nanopore centerline. In the limit of complete Debye overlap, this corresponds to the formation of a local Donnan equilibrium between the ends of the nanotube and the adjacent reservoirs.[1,11,16,27]

With the above boundary conditions, we can directly integrate eq 33 for the solute flux

$$\left(\frac{Du_R}{Du_L} + 1\right)\frac{J}{2\pi} = \left(\frac{Du_R}{Du_L} - 1\right) + 2Du_R\left[\ln\left(\frac{Du_R}{Du_L}\right) + \Delta V\right] \tag{35}$$

where we have used eq 32 and the definitions of Du_L and Du_R to rewrite the result in terms of the maximum Dukhin number Du_R and the ratio $Du_R/Du_L \equiv c_L/c_R$.

Using eq 33, we solve for $cd\phi/dx$ in terms of J and dc/dx, insert the result into eq 34, and integrate. The result can be combined with eq 35 to obtain

$$\ln\left(\frac{Du_R}{Du_L}\right) + \Delta V = \left(1 + \frac{I}{J}\right) \times \ln\left[\frac{\frac{Du_R}{Du_L} + 2Du_R\left(1 - \frac{I}{J}\right)}{1 + 2Du_R\left(1 - \frac{I}{J}\right)}\right] \tag{36}$$

Equation 36 may be used to determine the applied voltage as a function of the ratio I/J for given values of Du_R and Du_R/Du_L, and the result can be combined with eq 35 to determine the solute flux and ionic current as a function of applied voltage. IV curves obtained using eqs 35 and 36 are plotted in Figure 4 for a fixed value of $Du_R = 1$ and several values of $Du_R/Du_L \equiv c_L/c_R \geq 1$.

Limiting Conductances. As anticipated, as $Du_R/Du_L \to 1$, representing equal reservoir concentrations, the IV curve
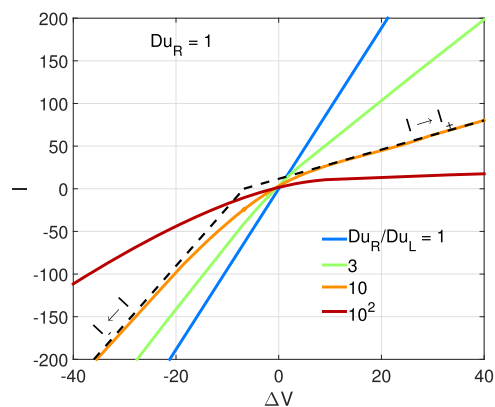

Figure 4. IV curves obtained from eqs 35 and 36 for a fixed value of $Du_R = 1$. The curves are colored according to $Du_R/Du_L \equiv c_L/c_R$ as indicated in the legend. The dashed black lines indicate I_+ and I_-, the currents obtained in the limit $\Delta V \to +\infty$ and $-\infty$, respectively, for $Du_R/Du_L = 10$ (see eqs 42 and 44.). The voltage is rescaled by the thermal voltage $k_B T/e \approx 25$ mV, and the current is rescaled according to Table 1.

becomes progressively more linear, and the conductance approaches a limiting value representing the sum of the bulk and surface electrophoretic contributions[1,9]

$$G = G_{bulk} + G_{surf} \tag{37}$$

with

$$G_{bulk} \equiv \pi \tag{38}$$

and

$$G_{surf} \equiv 2\pi Du_{ref} \tag{39}$$

This result is obtained by solving eqs 33 and 34 with $dc/dx = 0$. In dimensioned terms, these conductances are given by[9]

$$G_{bulk} = \frac{\pi R^2}{L}\frac{e^2 D}{k_B T}c_{res} \tag{40}$$

and

$$G_{surf} = \frac{2\pi R}{L}\frac{eD}{k_B T}|\sigma| \tag{41}$$

where c_{res} is the concentration in both reservoirs. This limiting conductance is indicated by the blue curve in Figure 4.

As a concentration difference is applied ($Du_R/Du_L > 1$) and increased, the IV curves become progressively more rectified. This is due to the asymmetry in selectivity between the left and right end of the nanotube. The Dukhin number at the right end is held fixed at one, resulting in substantial selectivity for positive coions at that end (Figure 1). On the other hand, as the Dukhin number on the left end is decreased via an increasing reservoir concentration c_L, the counterion selectivity at this end rapidly decreases, approaching the nonselective limit for values of $Du_R/Du_L > 10$ (Figure 1).

In order to fully understand under what conditions ICR occurs, we examine limiting voltage-independent conductances obtained under various conditions. We have already noted (eqs 37−41) the limiting conductance when the reservoir concentrations are equal ($Du_R/Du_L = 1$). We next examine the limiting currents and differential conductances $G \equiv \partial I/\partial \Delta V$ when Du_R and Du_R/Du_L are held fixed and $\Delta V \to \pm\infty$, denoted $I_\pm$ and $G_\pm$, respectively. From eq 36, we see that the logarithm on the right-hand side must diverge as the voltage

diverges for a fixed concentration ratio Du_R/Du_L. In the limit $|\Delta V| \to \infty$, the ionic current and solute flux will be in the same direction, such that the coefficient of the logarithm $1 + I/J > 0$. Thus, when $\Delta V \to +\infty$, the argument of the logarithm must diverge. This requires that $I/J \to 1 + (2Du_R)^{-1} \equiv STR_R^{-1}$, where STR_R is the STR at the right end of the nanopore (eq 23). Combined with eq 35, this gives for the current and conductance when $\Delta V \to +\infty$

$$\left(\frac{2\pi Du_{ref}}{STR_R}\right)^{-1} I_+ = \frac{1}{2Du_R}\left(\frac{Du_R}{Du_L} - 1\right) + \ln\left(\frac{Du_R}{Du_L}\right) + \Delta V$$
(42)

and

$$G_+ = \frac{G_{surf}}{STR_R} \equiv 2\pi Du_{ref} \frac{1 + 2Du_R}{2Du_R}$$
(43)

Likewise, as $\Delta V \to -\infty$, eq 36 indicates that the argument of the logarithm must vanish, and thus $I/J \to STR_L^{-1}$. By the same procedure we find

$$\left(\frac{2\pi Du_{ref}}{STR_L}\right)^{-1} I_- = \frac{1}{2Du_R}\left(\frac{Du_R}{Du_L} - 1\right) + \ln\left(\frac{Du_R}{Du_L}\right) + \Delta V$$
(44)

and

$$G_- = \frac{G_{surf}}{STR_L} \equiv 2\pi Du_{ref} \frac{1 + 2Du_L}{2Du_L}$$
(45)

These limiting currents are indicated in Figure 4 for $Du_R = 1$ and $Du_R/Du_L = 10$.

As Du_R becomes smaller for a fixed value of the ratio Du_R/Du_L, the voltage magnitude that leads to significant concentration accumulation or depletion becomes larger. This is because the asymmetry in nanopore selectivity between either end of the nanopore becomes weaker (Figure 1). This means that, for an experimentally feasible range of applied voltages, the IV curve linearizes as Du_R is decreased. From eq 36, we see that as $Du_R \to 0$ for a fixed value of Du_R/Du_L, $I/J \to \Delta V/\ln(Du_R/Du_L)$. This is true so long as the numerator and denominator of the logarithm are $\gg 0$, which, from our discussion above, requires that the voltage magnitude not be too large. We find from this limit and eq 35 a limiting conductance

$$G \to \frac{2\left(\frac{Du_R}{Du_L} - 1\right)}{\left(\frac{Du_R}{Du_L} + 1\right)\ln\left(\frac{Du_R}{Du_L}\right)} G_{bulk}$$
(46)

valid for fixed Du_R/Du_L when $Du_R \ll 1$. We note that the prefactor in eq 46 approaches unity and $G \to G_{bulk}$ in the limit $Du_R/Du_L \to 1$, as it must.

Finally, we examine the limit $Du_R \to \infty$ for fixed Du_R/Du_L. In this case, the entire nanopore becomes perfectly selective for counterions (Figure 1), and the IV curve again linearizes. Unlike in the case that $Du_R \ll 1$, however, we find that the IV curve is linear irrespective of the magnitude of the applied voltage for large Du_R. From eq 23, we note that, as $Du \to \infty$, $STR \to 1$. Thus, as $Du_R \to \infty$ for fixed Du_R/Du_L, $STR_L \to STR_R \to 1$, and, from eqs 43 and 45, we find $G_+ \to G_- \to G_{surf}$. In this case, the conductance is dominated by the (concentration-independent) surface contribution.

Each of the limiting conductances discussed above and the conditions under which they are obtained are listed in Table 2.

Table 2. Limiting Conductances for the Concentration Diode and the Conditions under Which They Are Obtained[a]

condition	G
$c_{max}/c_{min} = 1$	$G_{bulk} + G_{surf}$
$Du_{max} \ll 1$	$\dfrac{2(c_{max}/c_{min} - 1)}{(c_{max}/c_{min} + 1)\ln(c_{max}/c_{min})} \times G_{bulk}$
$Du_{max} \to \infty$	G_{surf}
$|\Delta V| \to \infty$	$G_{min} = \dfrac{1 + 2Du_{max}}{2Du_{max}} \times G_{surf}$
	$G_{max} = \dfrac{1 + 2Du_{min}}{2Du_{min}} \times G_{surf}$

[a]The results are written generically in terms of the maximum and minimum reservoir concentrations, c_{max} and c_{min}, respectively, and the corresponding maximum and minimum Dukhin numbers, $Du_{max} \equiv |\sigma|/ec_{min}R$ and $Du_{min} \equiv |\sigma|/ec_{max}R$, imposed on either end of the nanopore. G_{max} and G_{min} are, respectively, the maximum and minimum conductances obtained as $|\Delta V| \to \infty$. (see eqs 43, 45, 53, and 54.) The bulk (G_{bulk}) and surface (G_{surf}) electrophoretic conductances are given in eqs 38 and 39, respectively.

Rectification Ratio. We are now in a position to discuss the rectification ratio, defined as

$$\text{rectification ratio} \equiv \frac{|I(-|\Delta V|) - I(\Delta V = 0)|}{|I(+|\Delta V|) - I(\Delta V = 0)|}$$
(47)

We plot this ratio in Figure 5 as a function of Du_R for fixed concentration ratios $Du_R/Du_L = c_L/c_R$. In general, the
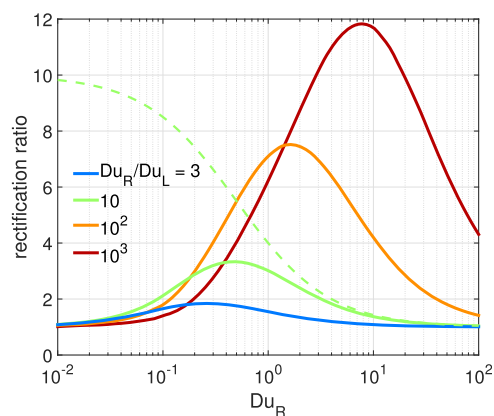

Figure 5. Rectification ratio obtained from eqs 35 and 36 and evaluated at $|\Delta V| = 40$ (≈ 1 V), as a function of Du_R. The curves are colored according to $Du_R/Du_L = c_L/c_R$ as indicated in the legend. The dashed line indicates the theoretical maximum rectification ratio, STR_R/STR_L, valid in the limit $|\Delta V| \to \infty$, for $Du_R/Du_L = 10$.

rectification ratio is a function of the voltage magnitude $|\Delta V|$; for definiteness, we take $|\Delta V| = 40$, which corresponds to a dimensioned applied voltage of approximately 1 V.

The rectification ratios display a peak for a finite value of Du_R (Figure 5). This peak grows and is shifted to higher values of Du_R as Du_R/Du_L is increased. The value of Du_R corresponding to the peak rectification ratio Du_R^{peak} is of order one over much of the parameter space ($0.2 < Du_R^{peak} < 2$ for $3 \leq Du_R/Du_L \leq 10^2$).

The fact that the rectification ratio shows a peak at a finite value of Du_R can be understood as follows: by taking the ratio of the limiting conductances valid when $|\Delta V| \to \infty$ (eqs 43 and 45), we see that there is an upper limit on the maximum rectification, given by $G_-/G_+ = STR_R/STR_L$ and valid in the limit $|\Delta V| \to \infty$. As $Du_R \to 0$ for a fixed value of Du_R/Du_L, this ratio reaches a maximum value equal to the concentration ratio Du_R/Du_L. However, in this case, the local Dukhin number is much smaller than 1 everywhere and the nanopore is therefore only weakly selective for counterions (Figure 1). It thus takes very large voltages to engender significant ion accumulation or depletion, voltages much larger than the practical upper limit in nanofluidic experiments (∼1 V), and the IV curve is effectively linearized.

On the other hand, when $Du_R \to \infty$ (with Du_R/Du_L fixed), $STR_R \to STR_L \to 1$, indicating that the IV curve is strictly linear in this limit, irrespective of the voltage magnitude. This is because the local Dukhin number is everywhere much larger than 1 and the entirety of the ionic transport is carried within the Debye layer. There is therefore no repartitioning of the transport between bulk and surface and no gradient in ion selectivity along the length of the nanopore. In this case, the conductance is given by the (concentration-independent) surface conductance (eq 41). Thus, the location of Du_R^{max} represents a compromise between the nonselective ($Du_R \to 0$) and perfectly selective ($Du_R \to \infty$) limits.

The occurrence of a maximum rectification ratio for a finite value of Du_R and a fixed value of the ratio Du_R/Du_L is exactly analogous to the common observation of a maximum rectification ratio for a finite concentration or surface charge density and a fixed geometry in conical diodes, for example, refs [4,5,14,15] In that case, the ratio of Dukhin numbers is fixed by the ratio of the base and tip radii, while the variation of the concentration or surface charge results in a variation of the maximum Dukhin number occuring at the tip of the conical nanopore. As in the concentration diode, the location of the maximum is determined by a compromise between the nonselective (high concentration or low surface charge) and perfectly selective (low concentration or high surface charge) limits. We will discuss the role of dynamic selectivity in diodes induced by asymmetric geometry (and surface charge density distributions) below.

Dynamic Selectivity and Limiting Conductances in Generic Diodes. *Rectification in Geometric and Concentration Diodes.* From our understanding of the role of the Dukhin number in controlling local selectivity, and of the mechanism of dynamic selectivity in controlling rectification, we conclude that ICR is generically a consequence of inequality of the Dukhin numbers imposed on either end of a nanopore, irrespective of whether that asymmetry is induced by a difference in reservoir concentrations, an asymmetric geometry, or an asymmetric surface charge density distribution (or any combination thereof). This is corroborated by the results shown in Figure 6, where we compare an IV curve obtained from the above solution for a concentration diode (eqs 35 and 36, Figure 6a,d) to numerical solutions of the transport equations (eqs 21 and 22) for the IV curve in a geometric (Figure 6b,e) and a charge diode (Figure 6c,f). In order to illustrate rectification induced by an asymmetric geometry, we assume a linear variation in the nanopore radius from the maximum radius (minimum Dukhin number) on the left to the minimum radius (maximum Dukhin number) on the right. The surface charge density is taken to be fixed and
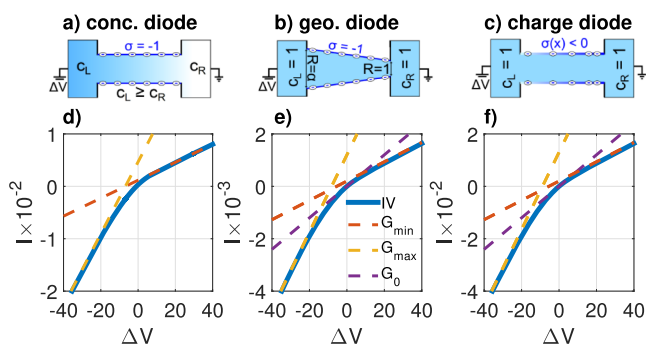

Figure 6. (a−c) Schematics of diodes induced by (a) unequal reservoir concentrations, (b) asymmetric geometry, and (c) asymmetric surface charge distribution. (d−f) IV curves obtained for $Du_R = 1$ and $Du_L = 0.1$ for (d) the concentration diode shown in (a), (e) geometric diode shown in (b), and (f) charge diode shown in (c). In panels (d−f), the dashed yellow and red lines show the maximum and minimum conductances obtained when $|\Delta V| \to \infty$ and calculated according to eqs 53 and 54, respectively. In panels (e,f), the dashed purple line indicates the linear response conductance valid in the vicinity of $\Delta V = 0$ for the charge and geometric diodes and calculated according to eq 63. The voltage is rescaled by the thermal voltage $k_B T/e \approx 25$ mV, and the current as well as the variables indicated in the schematics are rescaled according to Table 1.

negative, and the reservoir concentrations are taken to be equal. This configuration is shown schematically in Figure 6b.

Likewise, we illustrate rectification induced by a continuous, asymmetric surface charge profile by imposing a negative surface charge density whose magnitude varies linearly from a minimum density (minimum Dukhin number) on the left to a maximum density (maximum Dukhin number) on the right. In this case, we impose a constant nanopore radius and equal reservoir concentrations. This configuration is shown schematically in Figure 6c. In all three cases, we take $Du_L = 0.1$ and $Du_R = 1$. We immediately see from Figure 6d−f that the qualitative structure of the rectified IV curve is essentially the same over a given range of voltage ($-40 \leq \Delta V \leq +40$ here). Indeed, in each case, the rectification ratio (eq 47) is ∼3 for $|\Delta V| = 40$. The qualitative similarity of the IV curves obtained in these three different configurations illustrates the equivalence of the mechanism resulting in rectification.

General Expressions for the Limiting Conductances and Selectivities When $|\Delta V| \to \infty$. In this section, we show that the above expressions obtained for the limiting conductances when $|\Delta V| \to \infty$ (eqs 43 and 45) obtained for the concentration diode are particular examples of general expressions relating the minimum (maximum) Dukhin number imposed at one end of the nanopore to the maximum (minimum) conductance obtained for large imposed voltages. We also derive expressions for the limiting ion selectivities when $|\Delta V| \to \infty$. In the case of the geometric and charge diodes, these correspond to the minimum and maximum selectivities obtainable by varying the applied voltage. These expressions are valid for concentration, geometric, and charge diodes (or any combination thereof), as illustrated in Figure 6 for the limiting conductances. In the course of this discussion, we illustrate general features of the evolution of the Dukhin number profile in the nanopore interior as a function of applied voltage, further illustrating the principal role of dynamic selectivity in the accumulation or depletion of concentration in the nanopore interior and hence in ICR.

The general expressions for limiting conductances in generic diodes, along with those derived below for the linear response near $\Delta V = 0$ in geometric and charge diodes, will allow observations of rectified IV curves to be related to, for example, the surface charge density. The surface charge density is difficult to estimate directly and is often estimated by observing the saturation of the conductance at the surface-dominated value for low concentrations, for example, refs.[38,41,42] However, the inference of surface charge from conductance measurements typically relies on a linear response, in which case the relation between surface charge and the saturating conductance at low concentration is known analytically, for example, refs.[1,9,38] It is not clear a priori how this framework may be extended to, for example, conical nanopores, where ICR is inherent to the IV response below a certain concentration. To our knowledge, general analytical results for the relationship between surface charge and conductance do not exist in the literature for rectified IV curves, except in certain specialized scenarios, for example, ref 11.

Starting from eqs 21 and 22, we may write the transport equations generally as

$$\frac{J}{\pi R^2} = -\left[\frac{dc}{dx} + 2|Du|\left(\frac{dc}{dx} - Sc\frac{d\phi}{dx}\right)\right] \tag{48}$$

and

$$\frac{I}{\pi R^2} = -\left[c\frac{d\phi}{dx} - S2|Du|\left(\frac{dc}{dx} - Sc\frac{d\phi}{dx}\right)\right] \tag{49}$$

Note that we have assumed nothing about the sign of the surface charge S (except that it does not change along the length of the nanopore) or the nature of the variation of the local Dukhin number $|Du|$.

As $|\Delta V| \rightarrow \infty$, the solute flux will be dominated by the surface electrophoretic mass transport, $J/\pi R^2 \rightarrow S2|Du|c \, d\phi/dx = S2Du_{\text{ref}}(|\sigma|/R)d\phi/dx$. Integrating in x, we find

$$J = -S\left(\int_L \frac{dx}{2\pi R|\sigma|}\right)^{-1} Du_{\text{ref}}\Delta V \tag{50}$$

In order to obtain a condition on the flux ratio I/J that holds in the limit $|\Delta V| \rightarrow \infty$, we solve eqs 48 and 49 for the concentration gradient dc/dx in terms of I/J, the local Dukhin number, and the (divergent) solute flux

$$\frac{dc}{dx} = -S\frac{\frac{I}{J} + S\left(1 + \frac{1}{2|Du|}\right)}{2 + \frac{1}{2|Du|}}\frac{J}{\pi R^2} \tag{51}$$

On physical grounds, the concentration gradient cannot diverge everywhere in the nanopore interior, even in the limit that $|\Delta V| \rightarrow \infty$. Accordingly, the prefactor in eq 51 must vanish as the solute flux diverges. This requires that $I/J \rightarrow -S(1 + 1/2|Du|) \equiv -S/\text{STR}$, where in the second equality we have made use of eq 23. As the ratio I/J is spatially uniform at steady state, this condition requires the Dukhin number in the nanopore interior to approach a uniform value, which we will designate Du_u. Likewise, we designate the corresponding STR $\equiv u2Du_u/(1 + 2Du_u)$. With this result for the flux ratio I/J and eq 50, we find for the current

$$I = \left(\int_L \frac{dx}{2\pi R|\sigma|}\right)^{-1}\frac{Du_{\text{ref}}}{\text{STR}_u}\Delta V \tag{52}$$

The mechanism of concentration accumulation/depletion is driven by the gradient in the Dukhin number induced by the asymmetry between the maximum (Du_{max}) and minimum (Du_{min}) Dukhin numbers imposed on either end of the nanopore. Thus, for very strong applied voltages, the accumulation (depletion) will cease when the concentration everywhere is such that the uniform Dukhin number in the interior is equal to $Du_u = Du_{\text{min}}$ (Du_{max}). At one end of the nanopore, the concentration gradient then must diverge to match the divergence in the solute flux (eq 50) while allowing the Dukhin number to deviate from its uniform interior value and adjust to the appropriate boundary condition.

This mechanism is illustrated in Figure 7: in Figure 7a−c, we show the profiles of centerline concentration as a function of
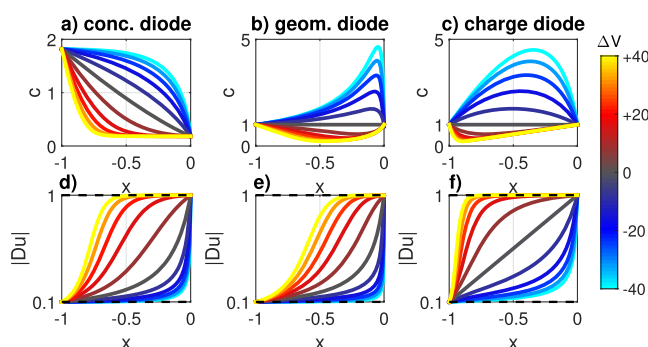

Figure 7. (a−c) Profiles of total ionic concentration along the length of the (a) concentration diode shown schematically in Figure 6a, (b) geometric diode (Figure 6b), and (c) charge diode (Figure 6c). (d−f) The corresponding profiles of the local Dukhin number for the concentration (d), geometric (e), and charge (f) diodes. The dashed black lines in (d−f) indicate the minimum and maximum imposed Dukhin numbers at either end of the nanopore, $Du_L = 0.1$ and $Du_R = 1$, respectively. In all panels, the curves are colored according to the applied voltage, as indicated in the colorbar on the right. The voltages are rescaled by the thermal voltage $k_BT/e \approx 25$ mV, and the concentrations are rescaled by the mean of the reservoir concentrations.

the applied voltage for the concentration (Figure 7a), geometric (Figure 7b), and charge (Figure 7c) diodes shown schematically in Figure 6a−c, respectively. In the case of the concentration diode, eq 51 may be integrated to obtain an implicit expression for the concentration profile, while for the geometric and charge diodes, it is necessary to solve the transport equations (eqs 21 and 22) numerically to obtain the concentration profiles. As for the IV curves shown in Figure 6d−f, the profiles are calculated for $Du_L = 0.1$ and $Du_R = 1$. The qualitative structure of the concentration profiles is quite different in the three configurations considered; however, in each case, there is increasing depletion (accumulation) of concentration in the nanopore interior for increasing magnitude positive (negative) voltage. Note that the sign of the voltage resulting in accumulation/depletion would be inverted for a positive surface charge, rather than the negative surface charge considered here.

However, in Figure 7d−f, we see that the evolution of the local Dukhin number profiles $|Du(x)|$ with applied voltage are strikingly similar in the three configurations, even though the concentration profiles are quite different. In each case, an increasing magnitude positive (negative) voltage results in a growing region in the nanopore interior where $|Du| \approx Du_{\text{max}} = Du_R$ ($|Du| \approx Du_{\text{min}} = Du_L$). Figure 7 illustrates the key role of

the local Dukhin number in controlling the accumulation/depletion of concentration in the nanopore and hence in ICR. It also illustrates that, in the extreme limit that $|\Delta V| \to \infty$, the Dukhin number will approach a uniform value equal to the maximum or minimum Dukhin number imposed at one end of the nanopore. (Whether it approaches Du_{max} or Du_{min} depends on the sign of the applied voltage and of the surface charge density.) Thus, denoting the maximum and minimum limiting conductances as G_{max} and G_{min}, respectively, we find

$$G_{max} = \frac{G_{surf}}{STR_{min}} \equiv G_{surf}\frac{1 + 2Du_{min}}{2Du_{min}} \tag{53}$$

and

$$G_{min} = \frac{G_{surf}}{STR_{max}} \equiv G_{surf}\frac{1 + 2Du_{max}}{2Du_{max}} \tag{54}$$

In these equations, G_{surf} is the surface conductance obtained when $Du_{ref} \to \infty$ and only the surface terms in eq 49 are relevant[43]

$$G_{surf} = \left(\int_L \frac{dx}{2\pi R|\sigma|}\right)^{-1} Du_{ref} \xrightarrow{\text{dim}} \frac{eD}{k_B T}\left(\int_L \frac{dx}{2\pi R|\sigma|}\right)^{-1} \tag{55}$$

where we have redimensionalized in the second line. The limiting conductances predicted using eqs 53 and 54 are shown in Figure 6d−f (dashed yellow and red lines).

We note that, by setting $|\sigma| \equiv R \equiv 1$ and identifying $Du_{min} = Du_L$ and $Du_{max} = Du_R$, we recover eqs 43 and 45 from eqs 54 and 53, respectively.

Figure 7d−f shows that the Dukhin number has not fully approached a uniform value everywhere in the nanopore interior even for $|\Delta V| = +40$; however, Figure 6d−f indicates that the differential conductance is roughly equal to its limiting value for $|\Delta V| \gtrsim 10-20$ (~250−500 mV). We note, however, that the voltage necessary to reach the limiting conductance depends on both the maximum Dukhin number in the system Du_{max} and the asymmetry in Dukhin numbers, quantified by the ratio Du_{max}/Du_{min} (see Figure 5 and related discussion). Thus, we note that care must be taken in applying eqs 53 and 54 to experimental *IV* curves. This difficulty can be avoided by instead fitting the surface charge to the linear response conductance G_0 obtained in the vicinity of $\Delta V = 0$; we will obtain an analytical expression for G_0 in the following section.

Using the asymptotic expressions for the solute flux (eq 50) and ionic current (eq 52−55), we can calculate the co-/counterion fluxes $J_{co/count} = (J \pm SI)/2$ and derive expressions for the counterion selectivities $S_{count} \equiv |J_{count}|/(|J_{co}| + |J_{count}|)$ in the limits $\Delta V \to \pm\infty$. The results are

$$S_{count}^{max} = \frac{1 + 4Du_{max}}{2 + 4Du_{max}} \quad \text{(reverse-bias)} \tag{56}$$

$$S_{count}^{min} = \frac{1 + 4Du_{min}}{2 + 4Du_{min}} \quad \text{(forward-bias)} \tag{57}$$

Equation 56 confirms eq 29. Furthermore, we see that the ionselectivity is maximized in the reverse-bias (low conductance) configuration, as previously noted. The coion selectivity is of course given by the relation $S_{co} + S_{count} = 1$.

Finally, before leaving this section, we derive eq 30 relating the conical conductance in the reverse-bias configuration to the conductance of a uniform nanopore having the same surface charge density and a constant radius equal to the tip radius. Equation 54 holds in the reverse-bias configuration. We perform the integration in eq 55 with $|\sigma| = 1$ and imposing a linear variation in the radius to find $G_{surf} = 2\pi Du_{tip}(\alpha - 1)/\ln \alpha$. We combine this result with eq 54, recognizing that $2\pi Du_{tip} \times (1 + 2Du_{tip})/2Du_{tip} = \pi + 2\pi Du_{tip} \equiv G_{uni}$, the uniform reference nanopore conductance (eq 37−39), to find

$$G_{min} = \frac{\alpha - 1}{\ln \alpha}G_{uni} \tag{58}$$

This confirms eq 30.

Conductance in the Vicinity of $\Delta V = 0$. In the case of the concentration diode, the imposed concentration difference means that there is a difference in electrochemical potentials between the reservoirs for at least one of the ionic species irrespective of the applied voltage. However, for the geometric and charge diodes equilibrium obtains when $\Delta V = 0$, and we can linearize about this equilibrium to obtain an expression for the differential conductance $G_0 \equiv \partial I/\partial\Delta V|_{\Delta V=0}$ in the vicinity of $\Delta V = 0$. The equilibrium state is characterized by $\Delta V = 0 \Rightarrow J_{co} = J_{count} = 0$ and the concentration, electrostatic potential, and electrochemical potential profiles $c \equiv 1$, $\phi \equiv 0$, and $\mu_{co} \equiv \mu_{count} \equiv -\ln 2$, respectively. We introduce a perturbative forcing $\delta V \ll 1$, which induces fluxes δJ_{co} and δJ_{count}. The applied voltage perturbs the concentration and electrostatic potential profiles such that $c \to 1 + c'$ and $\phi \to 0 + \phi'$, with $c' = 0$ on either end of the nanopore and ϕ' varying between δV on the left and 0 on the right end of the nanopore. The electrochemical potentials become $\mu_{co} \to -\ln 2 + c' + S\phi'$ and $\mu_{count} \to -\ln 2 + c' - S\phi'$, from which we define $\mu'_{co/count} \equiv c' \pm S\phi'$.

We linearize eqs 24 and 25 to find

$$\frac{\delta J_{co}}{\pi R^2} = -\frac{1}{2}\frac{d\mu'_{co}}{dx} \tag{59}$$

and

$$\frac{\delta J_{count}}{\pi R^2} = -\left(\frac{1}{2} + 2Du_{ref}\frac{|\sigma|}{R}\right)\frac{d\mu'_{count}}{dx} \tag{60}$$

Integration of eqs 59 and 60 along the length of the nanopore gives

$$\delta J_{co} = +S\frac{1}{2}\left(\int_L \frac{dx}{\pi R^2}\right)^{-1}\delta V \tag{61}$$

and

$$\delta J_{count} = -S\frac{1}{2}\left[\int_L \frac{dx}{\pi R^2(1 + 4Du_{ref}|\sigma|/R)}\right]^{-1}\delta V \tag{62}$$

From these results, we may calculate the conductance at $\Delta V = 0$ as $G_0 \equiv \delta I/\delta V \equiv S(\delta J_{co} - \delta J_{count})/\delta V$. We find

$$G_0 = \overbrace{\left(2\int_L \frac{dx}{\pi R^2}\right)^{-1}}^{G_0^{bulk}} + \underbrace{\left[2\int_L \frac{dx}{\pi R^2(1 + 4Du_{ref}|\sigma|/R)}\right]^{-1}}_{G_0^{surf}} \tag{63}$$

where we have partitioned the result into bulk and surface contributions. The conductances predicted from eq 63 are shown in Figure 6 for a diode induced by a linear variation in

(i) nanopore radius (Figure 6e) and (ii) surface charge density (Figure 6f).

For the sake of illustration, we derive an explicit expression for G_0 in a conical nanopore with a linearly varying radius and uniform surface charge density. Many studies have looked at ICR in such nanopores, for example, refs,[14−17,19,22−25,30,33] and our result will be useful in relating rectified IV curves to surface charge densities in conical nanopores.

We take the radius to vary linearly between a maximum at the base of the conical nanopore, R_{base}, and a minimum at the tip, R_{tip}. This gives for the magnitude of the radial slope $|dR/dx| = \alpha - 1$ (in rescaled variables), where $\alpha \equiv R_{base}/R_{tip}$, as introduced above. We insert this into eq 63, along with the condition that the surface charge density is uniform $|\sigma| = 1$, and evaluate the integrals to find

$$G_0^{bulk} = \pi \frac{\alpha}{2} \tag{64}$$

and

$$G_0^{surf} = \frac{\alpha - 1}{\ln\left(\frac{1 + 4Du_{tip}}{1 + 4Du_{tip}/\alpha}\right)} 2\pi Du_{tip} \tag{65}$$

In the above, we have recognized that $Du_{ref} = Du_{tip} \equiv |\sigma|/ec_{res}R_{tip}$, the Dukhin number defined in terms of the uniform surface charge density magnitude, reservoir concentration, and tip radius. Redimensioning eqs 64 and 65, we find

$$G_0^{bulk} = \frac{\pi R_{base} R_{tip}}{2L} \frac{e^2 D}{k_B T} c_{res} \tag{66}$$

and

$$G_0^{surf} = \frac{\alpha - 1}{\ln\left(\frac{1 + 4Du_{tip}}{1 + 4Du_{tip}/\alpha}\right)} \frac{2\pi R_{tip}}{L} \frac{eD}{k_B T} |\sigma| \tag{67}$$

Note that, in the limit of a uniform nanopore $\alpha \to 1$, the sum of eq 64 (66) and 65 (67) agrees with the sum of eq 38 (40) and 39 (41), as it must.

We find that the dependence of the surface conductance on the surface charge (through the terms proportional to Du_{tip} appearing in the logarithm) is more complicated than a linear proportionality, indicating that the results for the conductance in a conical nanopore reported in ref 43, for example, cannot be naively applied to the linear response conductance obtained for $|\Delta V| \ll k_B T/e$ (in dimensioned terms). The conductance derived in ref 43 indicates a linear proportionality between the surface conductance and the magnitude of the surface charge density, and we obtain the expression for the surface conductance given therein from eq 67 only in the limit that $4Du_{tip} \gg \alpha$.

■ DISCUSSION

Reanalysis of ICR Data in the Literature. Our results suggest that inequality of the Dukhin numbers imposed on either end of a nanopore is the only criterion for the occurrence of ICR. Further, they suggest that $Du \approx 1$ is a (rough) criterion for the maximization of rectification. To this end, we have reinterpreted data for conical nanopores in the literature in terms of the (maximal) tip Dukhin number (Table 3). We see that substantial rectification may be obtained even when the minimum radius is 2−3 orders of magnitude larger than the Debye length, but that peak rectification consistently

Table 3. Maximum Rectification Ratios in Conical Nanopores for Fixed Dukhin Ratios ($Du_{max}/Du_{min} = R_{base}/R_{tip}$) along with Corresponding Values of λ_D/R_{tip} and Du_{tip}, as Estimated from the Literature[a]

peak rect. ratio	λ_D/R_{tip}	Du_{tip}
10^{35}	$6(10^{-4})$	1.3
15^{36}	0.014	0.38
4.6^{15}	0.046	0.41
2.4^{12}	0.082	1.3
6.5^{25}	0.17	4.8
5.2^{15}	0.33	2.9
1.9^{24}	0.61	1.0

[a]The superscripts on the peak values of the rectification ratio indicate the corresponding reference. Note that the peak rectification ratios cannot be directly compared as they are not all calculated at the same reference voltage magnitude. (The reference voltage magnitudes range between 400 mV and 2 V.).

corresponds to $Du \approx 1$, consistent with our theoretical description of dynamic selectivity and its role in ICR.

In selecting experimental and numerical data from the literature, we searched for any rectification data that were obtained by imposing a continuous variation in concentration, geometry, and/or surface charge. Immediately, this excludes data obtained in charge diodes containing a discontinuity in the magnitude and/or sign of the surface charge, for example, refs.[18,26,32] The important distinction between diodes containing discontinuities in the local Dukhin number or the sign of the local surface charge and those considered here will be discussed in the following section. We additionally searched for rectification ratios (either directly reported or inferred from reported IV curves) that displayed a local maximum as the maximum Dukhin number was varied (via variations either in reservoir concentration or surface charge density) while the Dukhin ratio was held fixed. In the end, all of the data that fit our criteria were found to come from conical nanopores.

Note on the Distinction between Intrinsic and Extrinsic Diodes. Briefly, we note that we have been concerned here with the ICR induced by continuous variations in the local Dukhin number and in the presence of surface charge of a single sign. This is in contrast to both classical bipolar diodes, containing regions of both positive and negative surface charge, for example, refs,[11,16,18,30] and unipolar diodes, for example, refs.[20,26,32] containing regions of zero and nonzero surface charge. We term the latter intrinsic diodes, as in this case, the zone of depletion or accumulation is localized to the intrinsic discontinuity in either the local Dukhin number or the sign of the surface charge. We term the type of diodes considered here extrinsic diodes, in contrast to the previous terminology and in recognition of the fact that, in this case, the rectification is due to an imposed inequality in the Dukhin numbers on either end of the nanopore, rather than an intrinsic discontinuity.

Intrinsic diodes are typically found to exhibit much stronger rectification[26,30] because of the presence of a localized intrinsic accumulation/depletion zone. Picallo et al.[11] showed analytically that, in the limit of high surface charge ($Du \to \infty$), bipolar diodes exhibit ideal Shockley behavior, typical of classical p−n junction semiconductor diodes.[13] In this case, the current is described by $I = I_{sat}[1 - \exp(-e\Delta V/k_B T)]$, where I_{sat} is the finite saturation current obtained for large positive (reverse-biased) voltages. This is in strong contrast to the

behavior of extrinsic diodes as detailed above, in which two finite limiting conductances are observed for large positive or negative voltages, and it is further notable because it illustrates that rectification in intrinsic diodes is maximized as $Du \to \infty$, rather than being washed out.

■ CONCLUSIONS AND PERSPECTIVES

The principal conclusion of this work is that the key parameter controlling nanopore ion selectivity, through the mechanism of dynamic selectivity, is the Dukhin number $Du \equiv |\sigma|/ecR$; the ratio of the Debye length to nanopore radius λ_D/R is of secondary importance. As the Dukhin length $l_{Du} \equiv |\sigma|/ec$ can reach values of hundreds of nanometers for typical surface charge densities and ionic concentrations, this suggests that significant ionic selectivity can be obtained for large (10−100 nm) nanopores. This result has allowed us to rationalize the observation that significant ICR is routinely observed even when the nanopore radius is 1−3 orders of magnitude larger than the Debye length. In doing so, we have obtained several general formulae for limiting and linear response conductances in ionic diodes, which will allow researchers to relate *IV* measurements in asymmetric systems to unknown parameters such as the surface charge density.

Crucially, this mechanism suggests the possibility of designing large, conical pore ion-selective membranes. The tip radius and surface charge density of such membrane nanopores can be tailored to the operating concentrations in order to obtain significant ion selectivity (80−90%) while achieving orders-of-magnitude larger conductances than those obtained in traditional (subnanometric) ion-selective membranes. The implications for the design of much more efficient osmotic energy conversion (RED) and desalination/filtration (ED) devices is profound, as the key limiting factor in commercialization of such technologies is the poor efficiency due to low membrane conductance. Future work will focus on development of prototypical devices to demonstrate high-efficiency energy conversion and desalination in large nano-pores.

■ AUTHOR INFORMATION

Corresponding Author

*E-mail: lyderic.bocquet@lps.ens.fr

ORCID ◉

Anthony R. Poggioli: 0000-0002-0433-8127

Notes

The authors declare no competing financial interest.

■ ACKNOWLEDGMENTS

■ REFERENCES

(1) Bocquet, L.; Charlaix, E. Nanofluidics, from bulk to interfaces. *Chem. Soc. Rev.* **2010**, *39*, 1073−1095.

(2) Misakian, M.; Kasianowicz, J. J. Electrostatic Influence on Ion Transport through the aHL Channel. *J. Membr. Biol.* **2003**, *195*, 137−146.

(3) Schiedt, B.; Healy, K.; Morrison, A. P.; Neumann, R.; Siwy, Z. Transport of ions and biomolecules through single asymmetric nanopores in polymer films. *Nucl. Instrum. Methods Phys. Res., Sect. B* **2005**, *236*, 109−116.

(4) Vlassiouk, I.; Kozel, T. R.; Siwy, Z. S. Biosensing with nanofluidic diodes. *J. Am. Chem. Soc.* **2009**, *131*, 8211−8220.

(5) Zhou, K.; Perry, J. M.; Jacobson, S. C. Transport and sensing in nanofluidic devices. *Annu. Rev. Anal. Chem.* **2011**, *4*, 321−341.

(6) Siria, A.; Bocquet, M.-L.; Bocquet, L. New avenues for the large-scale harvesting of blue energy. *Nat. Rev. Chem.* **2017**, *1*, 0091.

(7) Rankin, D. J.; Huang, D. M. The effect of hydrodynamic slip on membrane-based salinity-gradient-driven energy harvesting. *Langmuir* **2016**, *32*, 3420−3432.

(8) Ren, Y.; Stein, D. Slip-enhanced electrokinetic energy conversion in nanofluidic channels. *Nanotechnology* **2008**, *19*, 195707.

(9) Siria, A.; Poncharal, P.; Biance, A.-L.; Fulcrand, R.; Blase, X.; Purcell, S. T.; Bocquet, L. Giant osmotic energy conversion measured in a single transmembrane boron nitride nanotube. *Nature* **2013**, *494*, 455−458.

(10) van der Heyden, F. H. J.; Bonthuis, D. J.; Stein, D.; Meyer, C.; Dekker, C. Electrokinetic energy conversion efficiency in nanofluidic channels. *Nano Lett.* **2006**, *6*, 2232−2237.

(11) Picallo, C. B.; Gravelle, S.; Joly, L.; Charlaix, E.; Bocquet, L. Nanofluidic osmotic diodes: Theory and molecular dynamics simulations. *Phys. Rev. Lett.* **2013**, *111*, 244501.

(12) Jubin, L.; Poggioli, A.; Siria, A.; Bocquet, L. Dramatic pressure-sensitive ion conduction in conical nanopores. *Proc. Natl. Acad. Sci. U.S.A.* **2018**, *115*, 4063−4068.

(13) Shockley, W. The Theory of p-n Junctions in Semiconductors and p-n Junction Transistors. *Bell Labs Tech. J.* **1949**, *28*, 435−489.

(14) Ai, Y.; Zhang, M.; Joo, S. W.; Cheney, M. A.; Qian, S. Effects of electroosmotic flow on ionic current rectification in conical nanopores. *J. Phys. Chem. C* **2010**, *114*, 3883−3890.

(15) Cervera, J.; Schiedt, B.; Neumann, R.; Mafé, S.; Ramírez, P. Ionic conduction, rectification, and selectivity in single conical nanopores. *J. Chem. Phys.* **2006**, *124*, 104706.

(16) Constantin, D.; Siwy, Z. S. Poisson-Nernst-Planck model of ion current rectification through a nanofluidic diode. *Phys. Rev. E: Stat., Nonlinear, Soft Matter Phys.* **2007**, *76*, 041202.

(17) Liu, Q.; Wang, Y.; Guo, W.; Ji, H.; Xue, J.; Ouyang, Q. Asymmetric properties of ion transport in a charged conical nanopore. *Phys. Rev. E: Stat., Nonlinear, Soft Matter Phys.* **2007**, *75*, 051201.

(18) Nguyen, G.; Vlassiouk, I.; Siwy, Z. S. Comparison of bipolar and unipolar ionic diodes. *Nanotechnology* **2010**, *21*, 265301.

(19) Siwy, Z.; Fuliński, A. Fabrication of a synthetic nanopore ion pump. *Phys. Rev. Lett.* **2002**, *89*, 198103.

(20) Wang, X.; Xue, J.; Wang, L.; Guo, W.; Zhang, W.; Wang, Y.; Liu, Q.; Ji, H.; Ouyang, Q. How the geometric configuration and the surface charge distribution influence the ionic current rectification in nanopores. *J. Phys. D: Appl. Phys.* **2007**, *40*, 7077−7084.

(21) Kubeil, C.; Bund, A. The role of nanopore geometry for the rectification of ionic currents. *J. Phys. Chem. C* **2011**, *115*, 7866−7873.

(22) Lan, W.-J.; Holden, D. A.; White, H. S. Pressure-dependent ion current rectification in conical-shaped glass nanopores. *J. Am. Chem. Soc.* **2011**, *133*, 13300−13303.

(23) Laohakunakorn, N.; Keyser, U. F. Electroosmotic flow rectification in conical nanopores. *Nanotechnology* **2015**, *26*, 275202.

(24) White, H. S.; Bund, A. Ion current rectification at nanopores in glass membranes. *Langmuir* **2008**, *24*, 2212−2218.

(25) Kovarik, M. L.; Zhou, K.; Jacobson, S. C. Effect of conical nanopore diameter on ion current rectification. *J. Phys. Chem. B* **2009**, *113*, 15960−15966.

(26) Li, C.-Y.; Ma, F.-X.; Wu, Z.-Q.; Gao, H.-L.; Shao, W.-T.; Wang, K.; Xia, X.-H. Solution-pH-modulated rectification of ionic current in highly ordered nanochannel arrays patterned with chemical functional

groups at designed positions. *Adv. Funct. Mater.* **2013**, *23*, 3836−3844.

(27) Vlassiouk, I.; Smirnov, S.; Siwy, Z. Nanofluidic ionic diodes. Comparison of analytical and numerical solutions. *ACS Nano* **2008**, *2*, 1589−1602.

(28) Cheng, L.-J.; Guo, L. J. Rectified ion transport through concentration gradient in homogeneous silica nanochannels. *Nano Lett.* **2007**, *7*, 3165−3171.

(29) Perry, J. M.; Zhou, K.; Harms, Z. D.; Jacobson, S. C. Ion transport in nanofluidic funnels. *ACS Nano* **2010**, *4*, 3897−3902.

(30) Vlassiouk, I.; Siwy, Z. S. Nanofluidic diode. *Nano Lett.* **2007**, *7*, 552−556.

(31) White, R. J.; Zhang, B.; Daniel, S.; Tang, J. M.; Ervin, E. N.; Cremer, P. S.; White, H. S. Ionic Conductivity of the Aqueous Layer Separating a Lipid Bilayer Membrane and a Glass Support. *Langmuir* **2006**, *22*, 10777−10783.

(32) Karnik, R.; Duan, C.; Castelino, K.; Daiguji, H.; Majumdar, A. Rectification of ionic current in a nanofluidic diode. *Nano Lett.* **2007**, *7*, 547−551.

(33) Woermann, D. Electrochemical transport properties of a cone-shaped nanopore: high and low electrical conductivity states depending on the sign of an applied electrical potential difference. *Phys. Chem. Chem. Phys.* **2003**, *5*, 1853−1858.

(34) Cheng, L.-J.; Guo, L. J. Nanofluidic diodes. *Chem. Soc. Rev.* **2010**, *39*, 923−938.

(35) He, X.; Zhang, K.; Li, T.; Jiang, Y.; Yu, P.; Mao, L. Micrometer-scale ion current rectification at polyelectrolyte brush-modified micropipets. *J. Am. Chem. Soc.* **2017**, *139*, 1396−1399.

(36) Lin, C.-Y.; Yeh, L.-H.; Siwy, Z. S. Voltage-induced modulation of ionic concentrations and ion current rectification in mesopores with highly charged pore walls. *J. Phys. Chem. Lett.* **2018**, *9*, 393−398.

(37) Vlassiouk, I.; Smirnov, S.; Siwy, Z. Ionic selectivity of single nanochannels. *Nano Lett.* **2008**, *8*, 1978−1985.

(38) Stein, D.; Kruithof, M.; Dekker, C. Surface-charge-governed ion transport in nanofluidic channels. *Phys. Rev. Lett.* **2004**, *93*, 035901.

(39) Plecis, A.; Schoch, R. B.; Renaud, P. Ionic transport phenomena in nanofluidics: Experimental and theoretical study of the exclusion-enrichment effect on a chip. *Nano Lett.* **2005**, *5*, 1147−1155.

(40) Fair, J. C.; Osterle, J. F. Reverse electrodialysis in charged capillary membranes. *J. Chem. Phys.* **1971**, *54*, 3307−3316.

(41) Karnik, R.; Castelino, K.; Fan, R.; Yang, P.; Majumdar, A. Effects of biological reactions and modifications on conductance of nanofluidic channels. *Nano Lett.* **2005**, *5*, 1638−1642.

(42) Secchi, E.; Niguès, A.; Jubin, L.; Siria, A.; Bocquet, L. Scaling behavior for ionic transport and its fluctuations in individual carbon nanotubes. *Phys. Rev. Lett.* **2016**, *116*, 154501.

(43) Frament, C. M.; Dwyer, J. R. Conductance-based determination of solid-state nanopore size and shape: An exploration of performance limits. *J. Phys. Chem. C* **2012**, *116*, 23315−23321.